Mitigation of Alfvén Activity in a Tokamak by Externally Applied Static 3D Fields

A. Bortolon,[1,2,*] W. W. Heidbrink,[1] G. J. Kramer,[3] J.-K. Park,[3] E. D. Fredrickson,[3] J. D. Lore,[4] and M. Podestà[3]

[1]*Department of Physics and Astronomy, University of California, Irvine, California 92697, USA*
[2]*Department of Nuclear Engineering, University of Tennessee, Knoxville, Tennessee 37996, USA*
[3]*Princeton Plasma Physics Laboratory, Princeton, New Jersey 08543, USA*
[4]*Oak Ridge National Laboratory, Oak Ridge, Tennessee 37831, USA*

(Received 15 February 2013; published 28 June 2013)

The application of static magnetic field perturbations to a tokamak plasma is observed to alter the dynamics of high-frequency bursting Alfvén modes that are driven unstable by energetic ions. In response to perturbations with an amplitude of $\delta B/B \sim 0.01$ at the plasma boundary, the mode amplitude is reduced, the bursting frequency is increased, and the frequency chirp is smaller. For modes of weaker bursting character, the magnetic perturbation induces a temporary transition to a saturated continuous mode. Calculations of the perturbed distribution function indicate that the 3D perturbation affects the orbits of fast ions that resonate with the bursting modes. The experimental evidence represents an important demonstration of the possibility of controlling fast-ion instabilities through "phase-space engineering" of the fast-ion distribution function, by means of externally applied perturbation fields.

DOI: 10.1103/PhysRevLett.110.265008 PACS numbers: 52.55.Fa, 52.25.Fi, 52.35.Bj, 52.55.Tn

In fusion devices such as tokamaks, charged fusion products need to be confined long enough to transfer their energy to the background plasma. Rapid losses induced by Alfvén instabilities may jeopardize performance or damage vessel hardware [1,2]. To avoid concentrated losses or unfavorable redistribution, methods are needed that suppress instability or mitigate its impact (without appreciable reduction in performance). The goal of mitigation is to control the nonlinear evolution of a dangerous instability, generally by limiting the size of the most violent events. For example, three-dimensional magnetic perturbation (MP) fields can mitigate or suppress edge localized modes (ELMs) [3] and electron cyclotron waves can reduce the amplitude and increase the frequency of sawtooth crashes [4].

Bursting, frequency-chirping modes driven by energetic particles are extremely common [5,6]. Examples span multiple frequency bands (from low frequency to ion cyclotron frequencies), confinement geometries (tokamaks, spherical tokamaks, and stellarators), and energetic-particle populations (beams, ion-cyclotron heating, and energetic electrons). Coupled "avalanches" of multiple bursting modes are also observed [7], in many cases accompanied by substantial fast ion losses.

The clearest published example of mitigation of an energetic-particle driven instability is an experiment performed in a small magnetic dipole device [8,9]. Application of electron cyclotron waves to the energetic electrons that were driving violent, bursting, rapidly chirping interchange modes converted the instability into a smaller amplitude mode of nearly constant frequency.

This Letter reports the first observation of mitigation of fast-ion driven, rapidly chirping Alfvénic modes. The application of static, three-dimensional MP fields modifies the nonlinear behavior of the Alfvénic modes.

The measurements are performed in the National Spherical Torus Experiment (NSTX) [10]. The fast ions that drive the instability are produced by injection of 90-keV deuterium neutrals into an ELM-free H-mode plasma with lithium-coated carbon walls [11]. Traces from two representative discharges ($I_p = 900$ kA, $B_t = 0.35$ T) appear in Fig. 1. During the flattop phase, the beam power and plasma current are constant, while the electron density steadily increases from 4 to 8×10^{19} m^{-3}. NSTX is equipped with a system of six two-turn coils that produce static magnetic-field perturbations. In discharge 138146, a configuration with toroidal periodicity $n = 3$ was employed and the coils were pulsed periodically. The MP pulses are 3 ms long and are applied at 20–40 Hz repetition rate, with coil current amplitude close to the threshold for repetitive triggering of ELM ("ELM pacing" [12]). In discharges such as the one shown in Fig. 1, ELM pacing does not occur, and the plasma remains virtually ELM free. The coil pulses cause rapid $\lesssim 10\%$ reductions in the volume-integrated neutron emission, whose secular decrease is associated with deuterium dilution from carbon accumulation. For these conditions, the neutron rate is dominated by beam-plasma reactions, so the reductions imply modest degradation of fast-ion confinement.

Persistent bursting modes at frequencies between 400–700 kHz are detected by magnetic probes in these discharges. The modes have toroidal mode numbers of $n = 7$–9 and, based on their mode numbers and frequency evolution [13] are thought to be global Alfvén eigenmodes (GAE) [14]. In the absence of MP fields, the modes chirp $\sim$100 kHz in frequency during each burst and the bursts occur at a repetition rate of $\sim$4 kHz (Fig. 2).

When the MP fields are applied, the frequency sweep, repetition period, and mode amplitude all drop by a factor

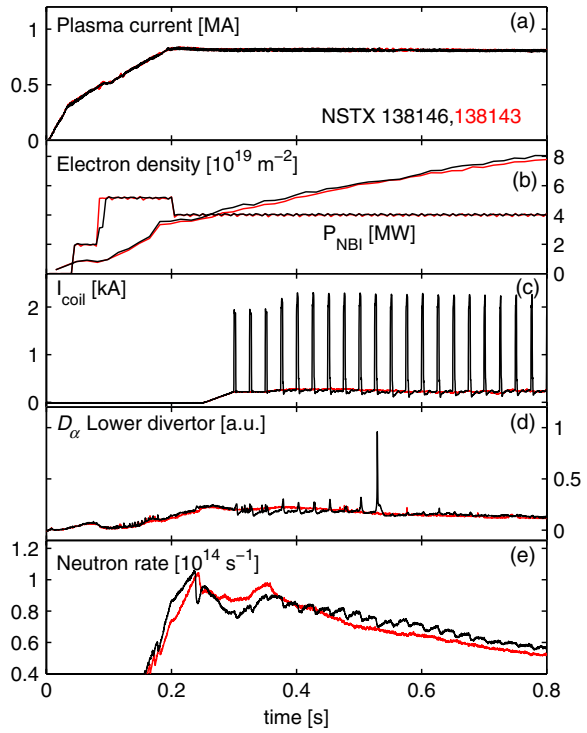

FIG. 1 (color online). Time evolution of (a) plasma current, (b) line-integrated electron density and beam power, (c) MP coil current per turn, (d) D_α emission from the divertor, and (e) volume-integrated neutron rate, in two discharges with $B_t = 0.35$ T, with (138146) and without (138143) applied MP.

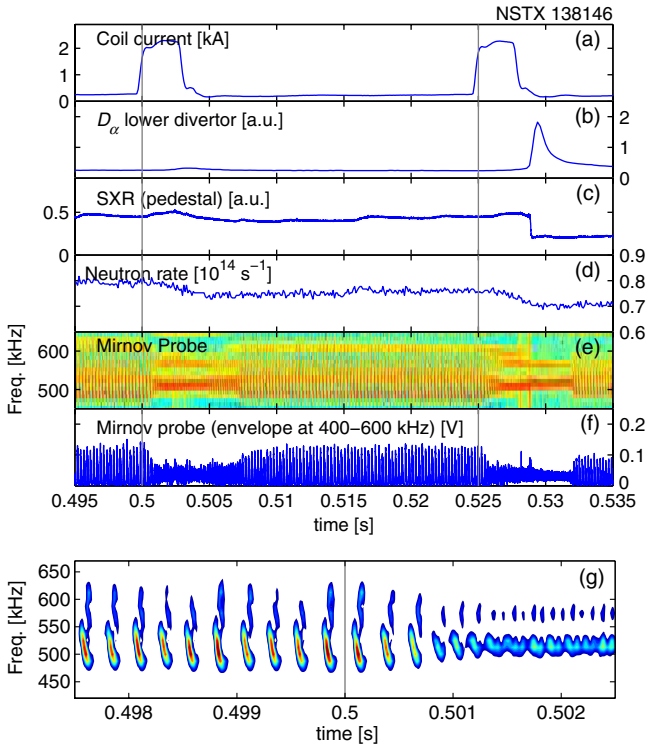

FIG. 2 (color online). Detail of the time evolution for the discharge with applied MP shown in Fig. 1. (a) MP coil current per turn, (b) D_α light, (c) soft x-ray emission from the plasma pedestal, (d) neutron rate, (e) spectrogram of high-frequency Alfvén activity from a magnetic coil, (f) bandpass-filtered and rectified magnetic-coil signal, and (g) detail of the chirping activity when the MP current turns on at $t = 0.5$ s.

of 2–3. The effect occurs in ~0.1 ms. This is a typical orbital time scale and is much shorter than the time scale for formation of the fast-ion population [$O(10)$ ms]. In contrast, when the MP current turns off, the bursting stays small for several milliseconds (i.e., the collisional time scale on which the fast-ion distribution function evolves). The mitigation effect is decoupled from ELM behavior and is most readily observed during ELM-free phases of the discharge. Edge soft x-ray signals are barely perturbed by the MP pulses, suggesting that the MP have a minor effect on plasma density and temperature profiles, so the associated changes in beam deposition cannot explain the phenomena.

As the density rises, the number of fast ions decreases and the GAE activity becomes less violent. In this phase of the discharge, in the absence of MP pulses, the activity [Figs. 3(a) and 3(b)] consists of single modes at ~540 kHz that have a modest frequency chirp of ~30 kHz, a repetition rate of 6 kHz, and a rise and decay time of 65 and 80 μs, respectively. When the $n = 3$ MP is applied, the instability transforms into a continuous mode with steady amplitude and frequency of 523 kHz [Figs. 3(c) and 3(d)]. Magnetic measurements indicate that the instability is an $n = 8$ mode that propagates opposite to the plasma current.

The phenomena shown in Figs. 2 and 3 are observed consistently in a database of 20 discharges of this type, with variable MP duration (2–6 ms), repetition rate (20–40 Hz), and coil current (0.8–2.2 kA per turn). Pulses with MP coil current below 1 kA per turn have little or no effect. Concurrent, large-amplitude, low-frequency MHD masks or weakens the mitigation effect.

In the Berk-Breizman model [15], rapid frequency chirping is associated with the formation of holes and clumps in fast-ion phase space. The resonant ions that drive the instability become trapped in the finite-amplitude wave. If a perturbation scatters the trapped fast ions out of resonance, it destroys the phase-space structures and suppresses the chirping. Although this model is a likely explanation for the mitigation of the fast-electron driven interchange mode [8,9], the persistence of the effect after the MP coil turns off suggests that a different mechanism is at work in this case. Apparently, the MP field quickly causes the loss of some of the fast ions that drive the instability, reducing the fast-ion drive for the instability. Then, after the perturbation is removed, the distribution function is gradually restored by the neutral beam source and strong nonlinear bursting resumes.

To investigate this hypothesis, we computed the fast-ion distribution function in the perturbed fields, using the full-orbit code SPIRAL [16]. SPIRAL calculates the orbits of test

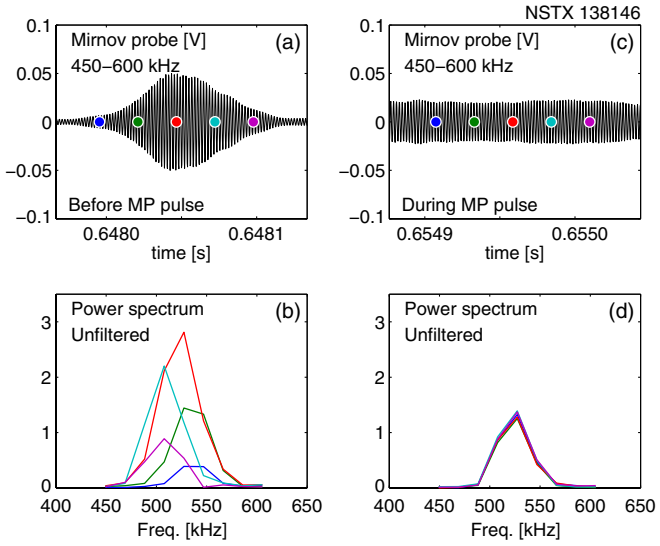

FIG. 3 (color online). Comparison of mode activity before (a) and during (c) MP fields, in the discharge of Fig. 1. Panels (a) and (c) show bandpass-filtered magnetic coil signals. Panel (b) shows power spectra computed at the times marked in panel (a); panel (d) shows power spectra at five different times for the continuous mode shown in panel (c).

particles in the equilibrium magnetic field accounting for collisional slowing down and pitch angle scattering. The particle birth location and velocity are provided by a beam attenuation code. The particles are loaded uniformly in time and followed for 35 ms, that is, longer than the energy slowing down time. The ensemble of the confined particles at this time represents the stationary distribution function. The simulation is then continued including the MP fields for another 10 ms time window, tracking the evolution of the distribution function each 0.02 ms.

The structure and amplitude of the perturbed fields is a delicate matter, especially in dynamic cases. The stationary vacuum fields $B^I_{\rm vac}$ at a given coil current I are calculated using Ampère's law and the realistic coil shapes. In response to external vacuum fields, the plasma develops internal currents that may screen out or amplify the fields. To assess this effect, the IPEC code [17] calculates the ideal plasma response to the $n = 3$ vacuum fields, $B^I_{\rm res}$. The total perturbed field is the sum of the vacuum and plasma fields $B^I_{\rm tot} = B^I_{\rm vac} + B^I_{\rm res}$. The radial component of the total perturbation field is shown in Fig. 4(a). The vacuum fields penetrate largely down to $R = 1.2$ m (approximately where the $q = 2$ surface is located). Partial field amplification results in structures that twist around the torus with $n = 3$ periodicity.

Another complication is that, in these experiments, the pulse duration is of the same order of the wall time constant, and due to the eddy currents in the wall, the vacuum field evolves without attaining the asymptotic nominal value. With a simplified approach, we express the vacuum field as $B_{\rm vac}(t) = A(t)B^I_{\rm vac}$. Since the ideal plasma response

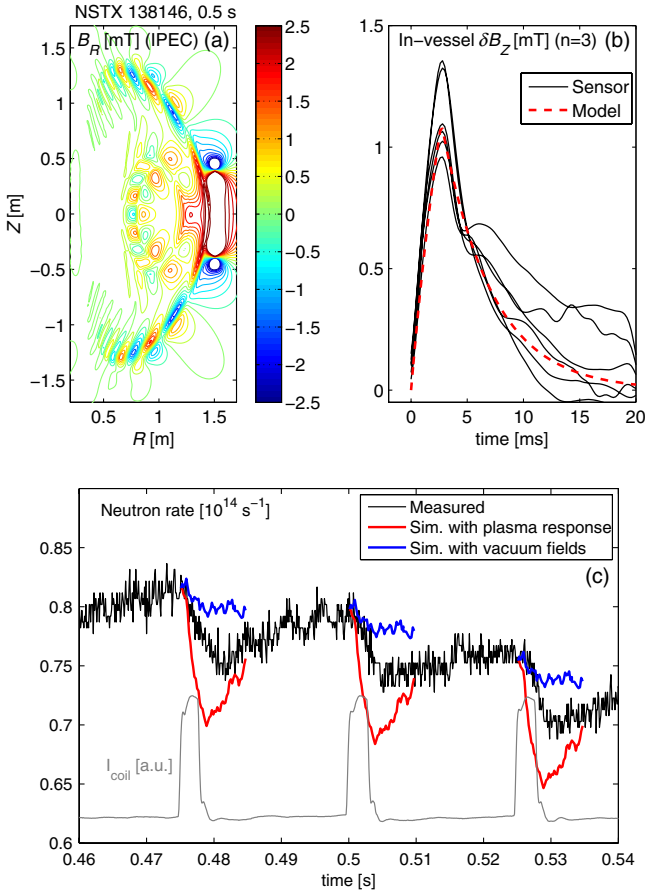

FIG. 4 (color online). (a) Radial component of the perturbed field at maximal amplitude including ideal plasma response to the perturbation, as computed by IPEC [17]. (b) Evolution of the perturbation field detected by an in-vessel magnetic sensor for a series of MP. (c) SPIRAL [16] calculation of the effect of the MP field on the neutron rate for a vacuum perturbation alone and including plasma response. The measured reduction lies between the vacuum and ideal-response calculations.

scales linearly with the vacuum field amplitude and is established on Alfvénic time scales (~ 10 μs), the total field is $B_{\rm tot}(t) = A(t)(B^I_{\rm vac} + B^I_{\rm res})$. The amplitude function $A(t)$ is derived taking as a reference the evolution of the poloidal field measured by a magnetic sensor, in the vacuum vessel, far from the plasma [Fig. 4(b)].

Figure 4(c) shows the effect on the neutron rate computed with vacuum fields only and including the plasma response. As expected, the actual neutron rate lies between these two extremes. The wall-shielding time constant described by $A(t)$ determines the rate of decay.

Figure 5 shows the calculated effect on the fast-ion distribution function $F(E, p)$ in velocity space. (Here, the energy E and pitch $p = v_\parallel/v$ are employed as coordinates and the values are taken at the particle location.) The unperturbed distribution function is a highly anisotropic slowing down distribution with peak at $p \approx 0.6$ [Fig. 5(a)]. Application of the MP alters the velocity-space distribution

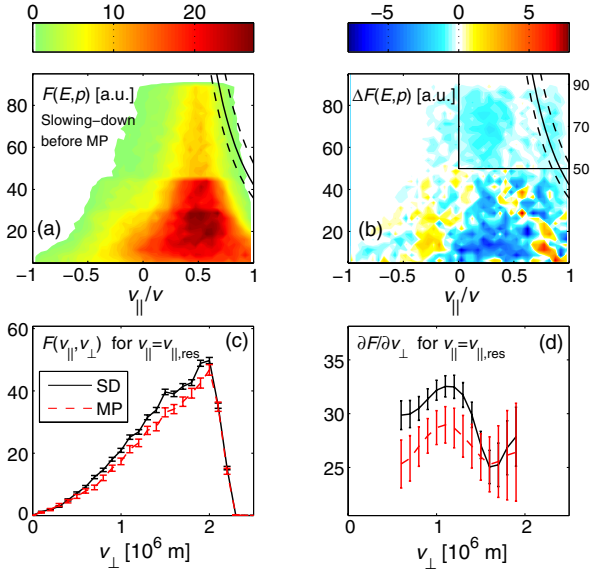

FIG. 5 (color online). Velocity space representation of the slowing-down (SD) distribution function $F(E, p)$ in the plasma core, as computed by SPIRAL (a) before the MP and (b) its variation after 1 ms from the application of the MP including plasma response. The curves overplotted indicate loci of possible resonance between fast ions and a mode at 520 ± 40 kHz. Lower values of F and $\partial F/\partial v_\perp$ along the resonance curve are found in the presence of MP (c), (d). Data in (c), (d) and in the inset of (b) are from simulations with enhanced statistical accuracy.

[Fig. 5(b)]. The MP depletes the number of fast ions with $0 < p < 0.6$ and $E < 50$ keV, while, for $E > 50$ keV, reductions occur for low ($p < 0.4$) and high ($p > 0.7$) pitch.

GAE instability is attributed to resonant fast ions. The resonance condition for GAE modes is

$$\omega = k_\parallel v_\parallel + l\omega_{ic}, \tag{1}$$

where ω is the wave frequency, $v_\parallel$ is the ion velocity component along the field line, ω_{ic} is the ion cyclotron frequency, and $k_\parallel$ is the parallel wave vector. The latter is related to the wave frequency in the dispersion relation for shear (torsional) Alfvén waves $\omega = k_\parallel v_A$, appropriate for GAE (v_A is the Alfvén velocity). For the observed GAEs, possible unstable resonances include direct $l = 0$ resonances in the core and in the plasma edge and a $l = 1$ Doppler-shifted cyclotron resonance in the plasma core. The MP alters the fast-ion distribution function at several of these candidate resonances. Figures 5(c) and 5(d) show the change for the core-localized Doppler-shifted cyclotron resonance, which lies on the flank of the calculated distribution function [Fig. 5(a)].

The statistical accuracy required to study the variation of F along the resonance was achieved by following a greater set of MC particles in the limited range $50 < E < 90$ keV [inset of Fig. 5(b)]. The population in the resonance region falls ~15% after application of the MP field [Fig. 5(c)]. For the vacuum MP alone, only a negligible change is predicted.

The instability of the mode depends in a complex way on the velocity space gradient of the distribution function along the resonance [14]. The profile of perpendicular velocity gradient $\partial F/\partial v_\perp$ along the resonance is plotted in Fig. 5(d). Simulations indicate a reduction of $\partial F/\partial v_\perp$ of the order of (10–20)%, suggesting a reduction of mode drive. A quantitative computation requires the knowledge of the spatial eigenfunction of the mode, which in previous NSTX studies of Alfvénic modes, could be obtained by validating MHD simulations on internal fluctuation measurements by reflectometry [18]. Unfortunately, the latter were not available in the present steep-pedestal discharges, precluding an accurate computation of the drive. Nevertheless, chirping and bursting dynamics are generally associated with conditions of marginal stability [15], hence changes such as this may engender the observed modification in nonlinear behavior.

Alternative explanations invoking an increased mode damping are considered unlikely. The main damping mechanisms (Landau damping and, in particular, continuum damping [14]) are determined by the characteristics of the kinetic equilibrium profiles. However, changes under the applied MP are smaller than those observed during the natural discharge evolution (for instance, at the onset of low frequency MHD or ELMs), which have generally little effect on the persistent GAE activity.

In conclusion, the reported results show that externally imposed 3D fields can alter the nonlinear evolution of a tokamak fast-particle driven instability. Full-orbit simulations, reproducing the observed evolution of neutron production rate, indicate that the MP fields can reduce the fast ion drive of the modes by depleting the number of resonant fast ions.

Although these NSTX high-frequency modes are not particularly detrimental to performance, the data presented here are an important early demonstration of the possibility of controlling fast-ion instabilities by "phase-space engineering" of the fast-ion distribution function. Through application of properly tailored static fields or propagating waves, mitigation of dangerous energetic-particle instabilities may be possible.

The authors thank the NSTX team for their support. This work was supported by the US DOE (Contracts No. DE-FG02-06ER54867, No. DE-AC02-09CH11466, and No. DOE-DE-SC0008309).

*abortolon@pppl.gov

[1] H. Duong, W. Heidbrink, E. Strait, T. Petrie, R. Lee, R. Moyer, and J. Watkins, Nucl. Fusion **33**, 749 (1993).
[2] R. B. White, E. Fredrickson, D. Darrow, M. Zarnstorff, R. Wilson, S. Zweben, K. Hill, Y. Chen, and G. Fu, Phys. Plasmas **2**, 2871 (1995).
[3] T. E. Evans, R. A. Moyer, P. R. Thomas, J. G. Watkins, T. H. Osborne, J. A. Boedo, E. J. Doyle, M. E. Fenstermacher,

K. H. Finken, R. J. Groebner *et al.*, Phys. Rev. Lett. **92**, 235003 (2004).
[4] I. T. Chapman, Plasma Phys. Controlled Fusion **53**, 013001 (2011).
[5] B. N. Breizman and S. E. Sharapov, Plasma Phys. Controlled Fusion **53**, 054001 (2011).
[6] W. W. Heidbrink, Phys. Plasmas **15**, 055501 (2008).
[7] M. Podestà, W. W. Heidbrink, D. Liu, E. Ruskov, R. E. Bell, D. S. Darrow, E. D. Fredrickson, N. N. Gorelenkov, G. J. Kramer, B. P. LeBlanc *et al.*, Phys. Plasmas **16**, 056104 (2009).
[8] D. Maslovsky, B. Levitt, and M. E. Mauel, Phys. Plasmas **10**, 1549 (2003).
[9] D. Maslovsky, B. Levitt, and M. E. Mauel, Phys. Rev. Lett. **90**, 185001 (2003).
[10] M. Ono, S. Kaye, Y.-K. Peng, G. Barnes, W. Blanchard, M. Carter, J. Chrzanowski, L. Dudek, R. Ewig, D. Gates *et al.*, Nucl. Fusion **40**, 557 (2000).
[11] R. Maingi, D. Boyle, J. Canik, S. Kaye, C. Skinner, J. Allain, M. Bell, R. Bell, S. Gerhardt, T. Gray *et al.*, Nucl. Fusion **52**, 083001 (2012).
[12] J. M. Canik, R. Maingi, T. E. Evans, R. E. Bell, S. P. Gerhardt, B. P. LeBlanc, J. Manickam, J. E. Menard, T. H. Osborne, J.-K. Park *et al.* (NSTX Team), Phys. Rev. Lett. **104**, 045001 (2010).
[13] N. A. Crocker, W. A. Peebles, S. Kubota, J. Zhang, R. E. Bell, E. D. Fredrickson, N. N. Gorelenkov, B. P. LeBlanc, J. E. Menard, M. Podestà *et al.*, Plasma Phys. Controlled Fusion **53**, 105001 (2011).
[14] N. Gorelenkov, E. Fredrickson, E. Belova, C. Cheng, D. Gates, S. Kaye, and R. White, Nucl. Fusion **43**, 228 (2003).
[15] H. L. Berk, B. N. Breizman, and M. Pekker, Phys. Rev. Lett. **76**, 1256 (1996).
[16] G. J. Kramer, R. V. Budny, A. Bortolon, E. D. Fredrickson, G. Y. Fu, W. W. Heidbrink, R. Nazikian, E. Valeo, and M. A. V. Zeeland, Plasma Phys. Controlled Fusion **55**, 025013 (2013).
[17] J.-K. Park, A. H. Boozer, and A. H. Glasser, Phys. Plasmas **14**, 052110 (2007).
[18] E. Fredrickson, N. Crocker, D. Darrow, N. Gorelenkov, G. Kramer, S. Kubota, M. Podesta, R. White, A. Bortolon, S. Gerhardt *et al.*, Nucl. Fusion **53**, 013006 (2013).